Literature Report

Reporter: Kang-Ming Xiong

Date: 2020-12-31

Introduction

nature COMMUNICATIONS

Article | Open Access | Published: 03 December 2020

Upconversion NIR-II fluorophores for mitochondria-targeted cancer imaging and photothermal therapy

Hui Zhou[1,2,7], Xiaodong Zeng[1,3,7], Anguo Li[1], Wenyi Zhou[1,3], Lin Tang[1], Wenbo Hu[4], Quli Fan[4], Xianli Meng[5], Hai Deng[6], Lian Duan[1], Yanqin Li[1], Zixin Deng[1], Xuechuan Hong[1,2✉] & Yuling Xiao[1,3✉]

个人简介

2010.10 – 至今 武汉大学药学院教授，博士生导师

研究领域

近红外二区有机小分子探针的制造，可视化肿瘤、病毒感染机制研究及药物开发

洪学传

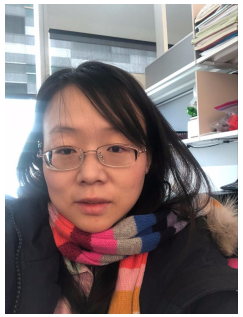

肖玉玲

个人简介

2012 -至今 武汉大学药学院讲师、副教授

研究领域

1）基于纳米医学技术的癌症早期诊断和治疗
2）小分子药物及核酸药物的靶向传输及控制释放研究

Introduction

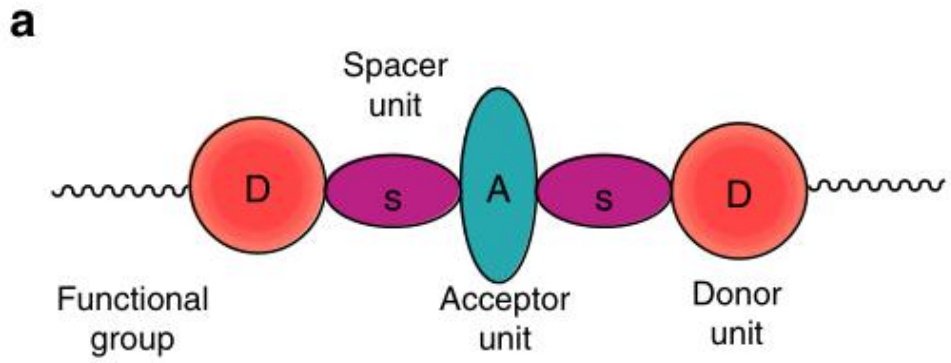

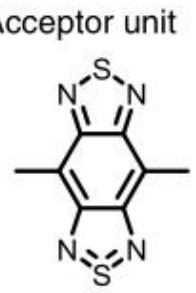

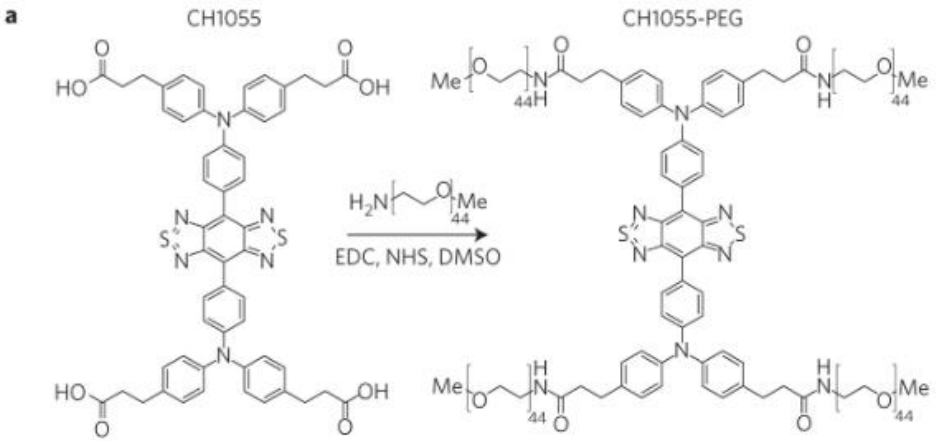

它们组第一个小分子有机NIR-II染料最初是由**苯并双(1,2,5-噻二唑)(BBTD)**形成的**CH1055**荧光团，该荧光团在~750 nm处吸收光，在~1055 nm处发光。

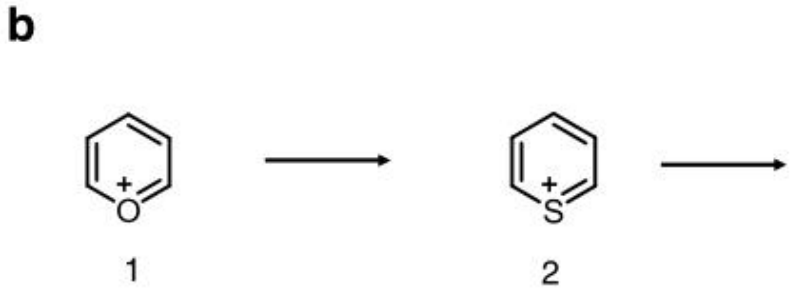

硫代吡啶的E_{gap}低于吡喃，这表明硫代吡咯盐可能成为新的近红外受体。

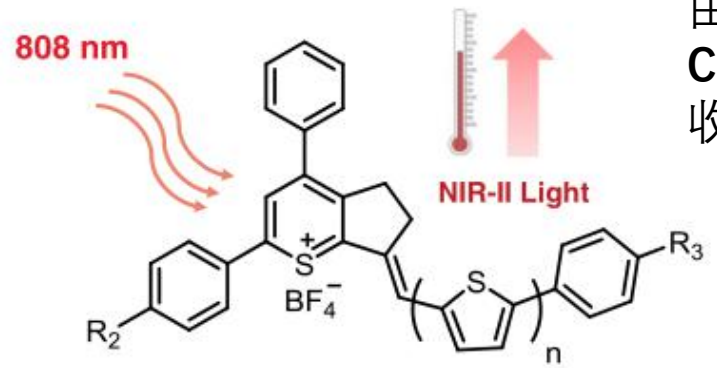

供体-受体(D-A)结构的新型红移噻吩染料

Fig. 1 Structural design and bright-filed images of 3a–3k, H4. a Traditional NIR-II small-molecule dyes based on the BBTD core with D–A–D or symmetrical structures. **b** A new strategy for the construction of D–A type thiopyrylium mitochondria-targeted NIR-II dyes with FUCL and photothermal properties, $n = 0, 1$. **c** Bright field images of a series of new thiopyrylium-based probes 3a–3k and H4 in dichloromethane.

Introduction

Compound	HOMO	Energy (eV)	LUMO	Energy (eV)	E_{gap} (eV)	Compound	HOMO	Energy (eV)	LOMO	Energy (eV)	E_{gap} (eV)
		-9.62		-4.03	5.59			-9.45		-4.09	5.37

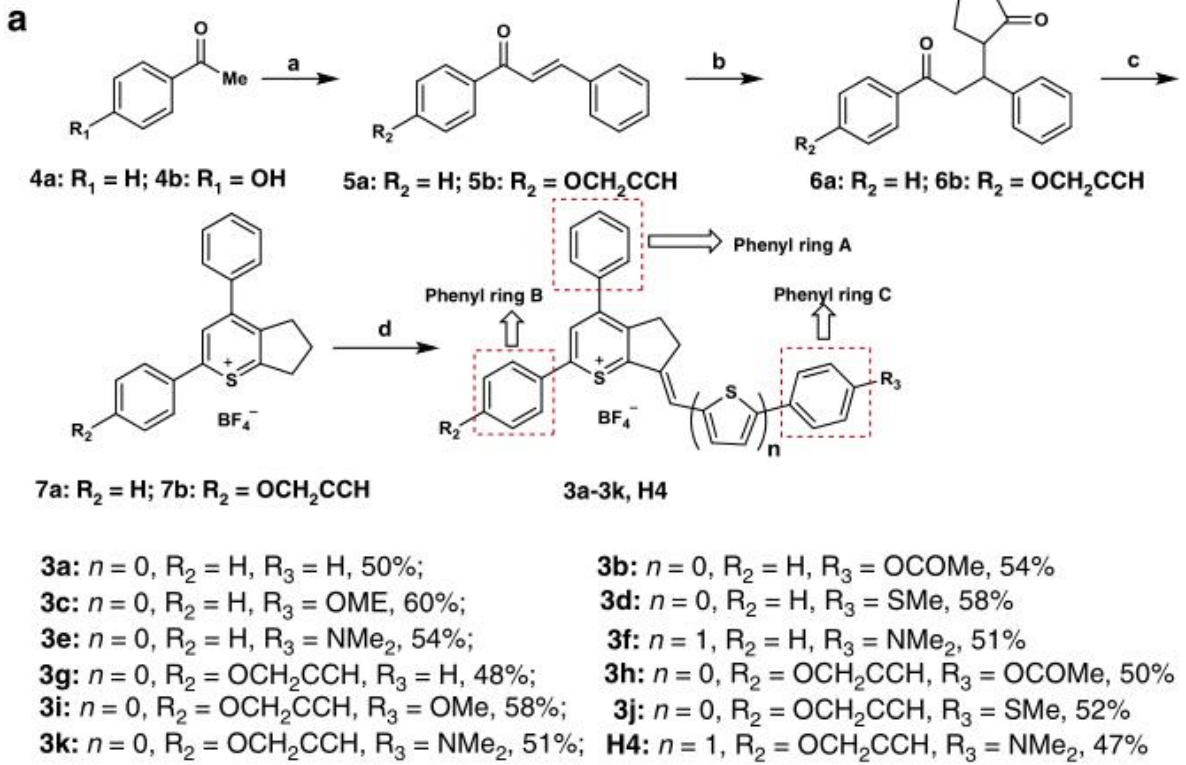

3a: $n = 0$, R_2 = H, R_3 = H, 50%;
3b: $n = 0$, R_2 = H, R_3 = OCOMe, 54%
3c: $n = 0$, R_2 = H, R_3 = OME, 60%;
3d: $n = 0$, R_2 = H, R_3 = SMe, 58%
3e: $n = 0$, R_2 = H, R_3 = NMe_2, 54%;
3f: $n = 1$, R_2 = H, R_3 = NMe_2, 51%
3g: $n = 0$, R_2 = OCH_2CCH, R_3 = H, 48%;
3h: $n = 0$, R_2 = OCH_2CCH, R_3 = OCOMe, 50%
3i: $n = 0$, R_2 = OCH_2CCH, R_3 = OMe, 58%;
3j: $n = 0$, R_2 = OCH_2CCH, R_3 = SMe, 52%
3k: $n = 0$, R_2 = OCH_2CCH, R_3 = NMe_2, 51%;
H4: $n = 1$, R_2 = OCH_2CCH, R_3 = NMe_2, 47%

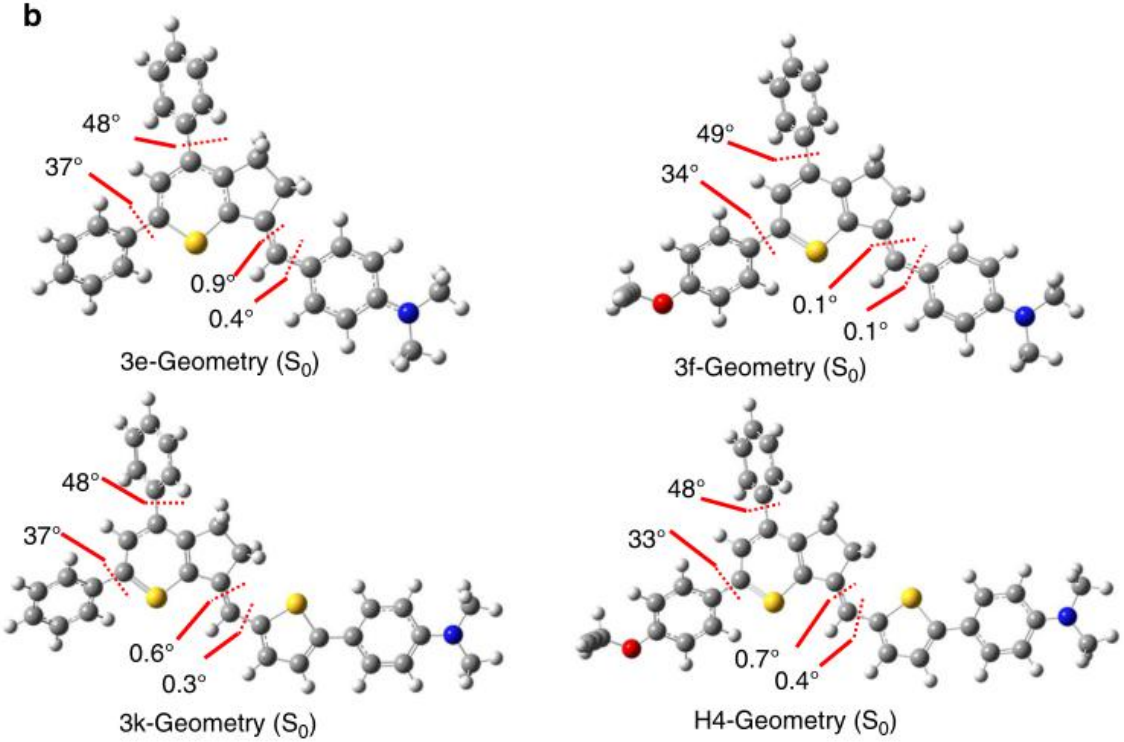

Fig. 2 Synthetic route of 3a–3k, H4 and the calculated optimized geometries of 3e–3k, H4. a Reagents and conditions: **a** (i) acetophenone, benzaldehyde, 3 M aqueous KOH, EtOH, 25 °C, 14 h, 5a: 80%; 1-(4-hydroxyphenyl)ethan-1-one: 82%; (ii) K_2CO_3, 3-bromoprop-1-yne, acetone, reflux 4 h, 5b: 97%; **b** (i) cyclopentanone, pyrrolidine, benzene, 100 °C, 4 h; (ii) compound 5, dioxane, reflux, 6 h, 6a: 68%; 6b: 66%; **c** thioacetic acid, boron trifluoride ether, ether, 60 °C, 2 h, 7a: 62%; 7b: 50%; **d** aldehydes, acetic anhydride, 70 °C, under microwave irradiation, 75 °C, 2 h, 47–60%. **b** Calculated optimized ground state (S_0) geometries of the molecules at the B3LYP/6-31 G (**d**) level (Gaussian 09, Revision D.09).

Introduction

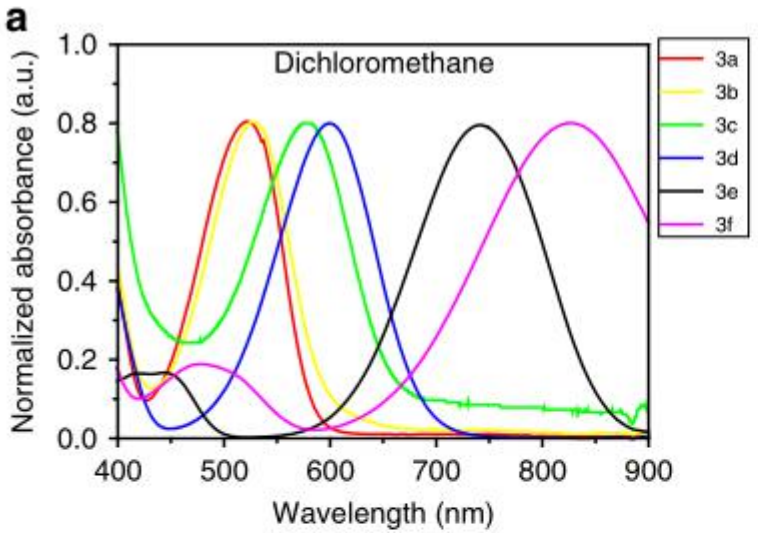

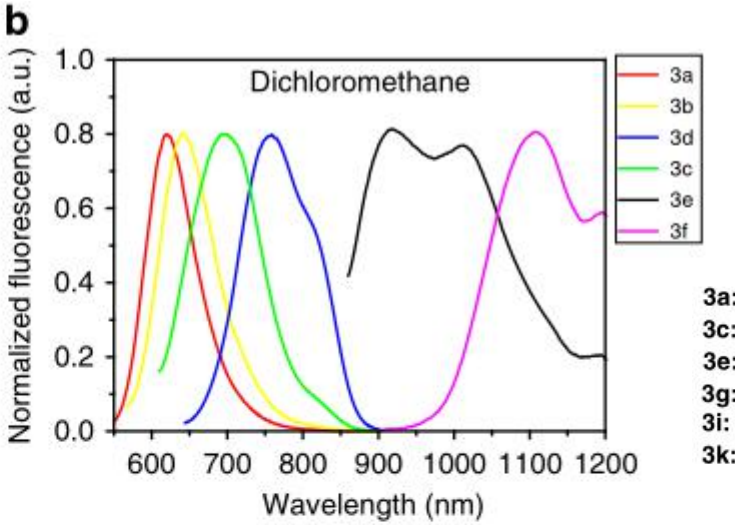

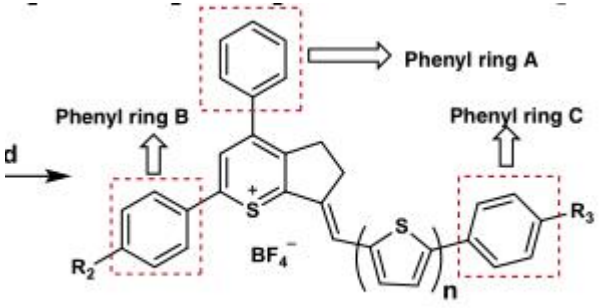

3a-3k, H4

3a: $n = 0$, $R_2 = H$, $R_3 = H$, 50%;
3b: $n = 0$, $R_2 = H$, $R_3 = OCOMe$, 54%
3c: $n = 0$, $R_2 = H$, $R_3 = OME$, 60%;
3d: $n = 0$, $R_2 = H$, $R_3 = SMe$, 58%
3e: $n = 0$, $R_2 = H$, $R_3 = NMe_2$, 54%;
3f: $n = 1$, $R_2 = H$, $R_3 = NMe_2$, 51%
3g: $n = 0$, $R_2 = OCH_2CCH$, $R_3 = H$, 48%;
3h: $n = 0$, $R_2 = OCH_2CCH$, $R_3 = OCOMe$, 50%
3i: $n = 0$, $R_2 = OCH_2CCH$, $R_3 = OMe$, 58%;
3j: $n = 0$, $R_2 = OCH_2CCH$, $R_3 = SMe$, 52%
3k: $n = 0$, $R_2 = OCH_2CCH$, $R_3 = NMe_2$, 51%;
H4: $n = 1$, $R_2 = OCH_2CCH$, $R_3 = NMe_2$, 47%

3f和H4的UV-Vis-NIR吸收带位于580-1100 nm，而3f和H4的荧光发射光谱在~1100 nm处出现峰值发射波长

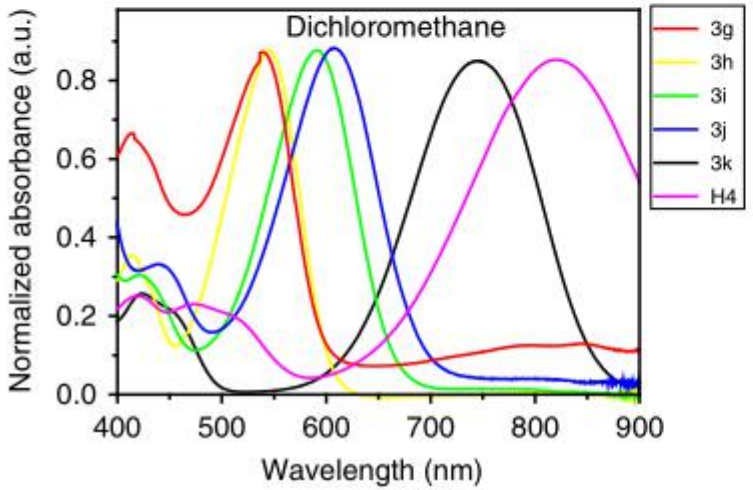

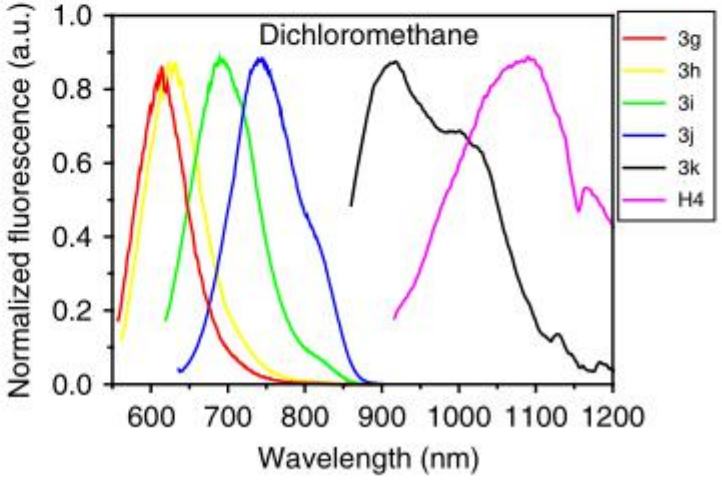

斯托克斯位移的大小与R_3上取代基的相对**给电子能力**一致。随着供体电子密度的增加，λ_{ex}和λ_{em}不断向更长的波长移动。如果以化合物3a或3g的R_3位H取代为参照，在R_3位引入OAc(3b，3h)、OMe(3c，3i)和SMe(3d，3j)等给电子取代基，可使荧光向NIR-I波长稳定红移15-130 nm，荧光量子产率可达31%。

Fig. 3 Spectroscopic properties of 3a-3k and H4. a Absorption wavelength and **b** emission wavelength of 3a-3f in dichloromethane. **c** Absorption wavelength and **d** emission wavelength of 3g-3k and H4 in dichloromethane.

Introduction

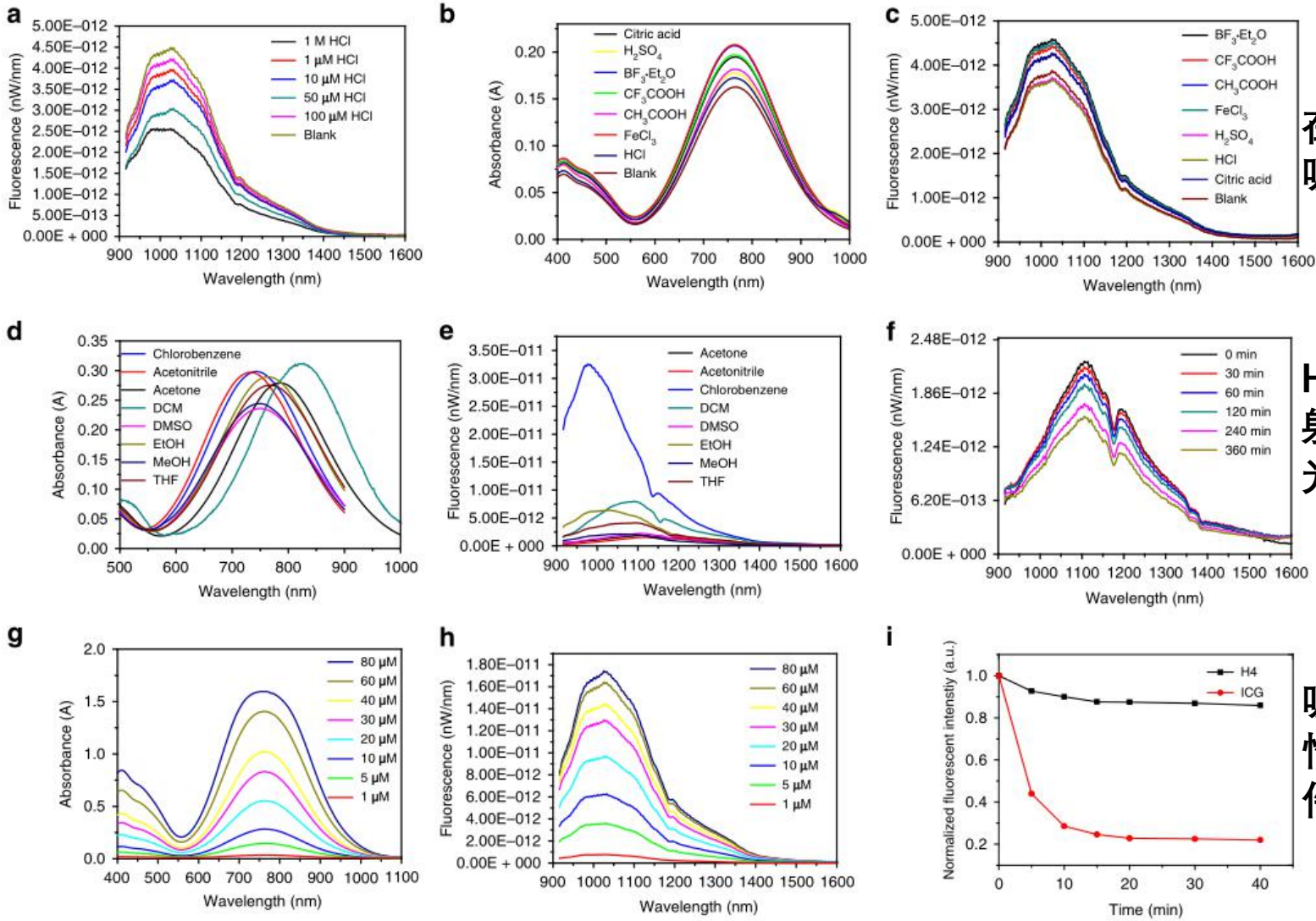

在不同酸性物质条件下，H4溶液的吸收波长和荧光发射波长保持不变。

H4在极性溶剂中表现出一个宽峰，发射明显猝灭，增加溶剂极性导致发射光谱向更长的波长移动。

吸光度和荧光随H4浓度的增加而线性增加(图4G，h)，表明在广泛的条件下没有聚集

Fig. 4 Spectroscopic properties of H4. a Fluorescent emission of H4 (10 μM) in EtOH with different concentrations of HCl. **b** Absorbance and **c** fluorescent emission of H4 in different acids. **d** Absorbance and **e** fluorescent emission of H4 in 10 μM different solvents. **f** Fluorescent intensity of H4 in DMSO at different times. **g** Absorbance and **h** fluorescent emission of H4 in EtOH with different concentrations. **i** Compared stability of H4 with ICG in DMSO under continuous 808 nm laser irradiation.

Introduction

寡肽PPSHTPT(PT)首次设计用于模拟体内天然蛋白骨钙素的性质，并对骨肉瘤细胞系(如143B细胞) 具有高度的亲和力和特异性。

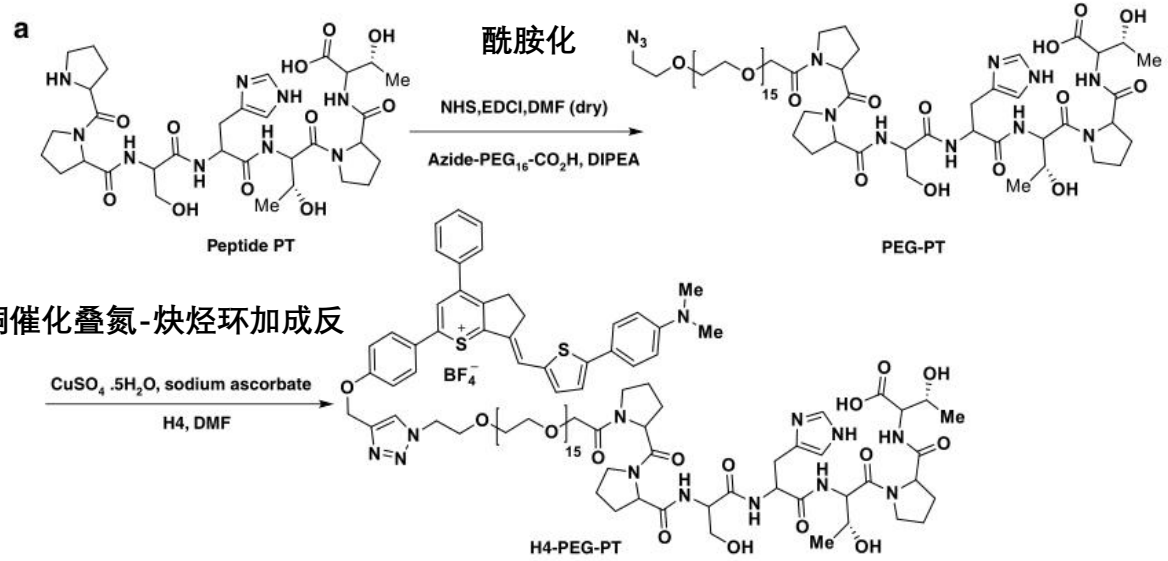

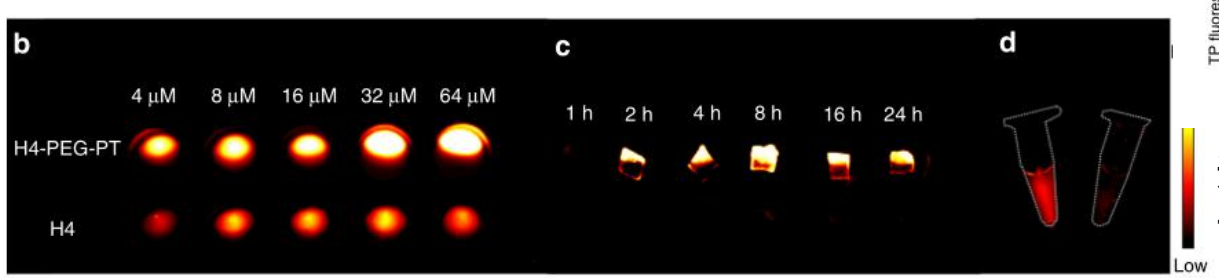

在体外的骨结合试验中，羟基磷灰石(HA)(10 mg)与不同浓度的H4-PEG-PT(4、8、16、32和64μM)孵育4h后，HA沉淀的荧光信号增强了。H4-PEG-PT对HA有很高的亲和力, 而在没有靶向配体PT的情况下，在不同浓度的H4的HA沉淀物中检测到强度低得多的荧光信号。

C: H4-PEG-PT孵育不同时间点的软骨切片的C荧光图像。
D:H4-PEG-PT(左)和H4-PEG-PT与过量PT作为竞争剂(右)标记的143B细胞在808 nm(1000lp，100ms)激发下的NIR-II信号。

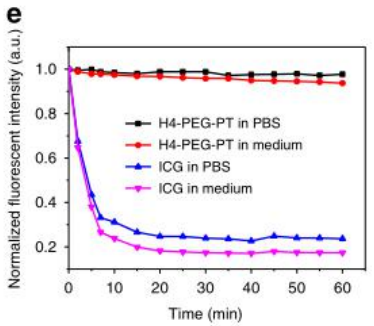

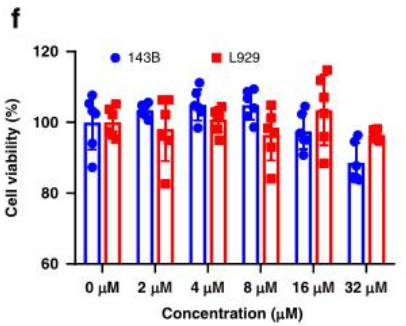

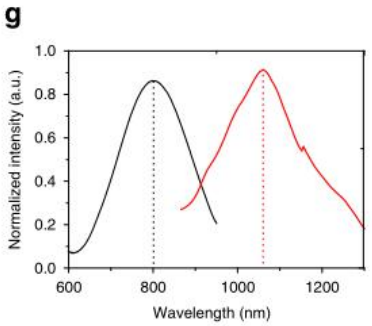

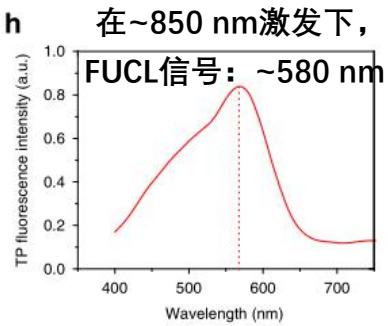

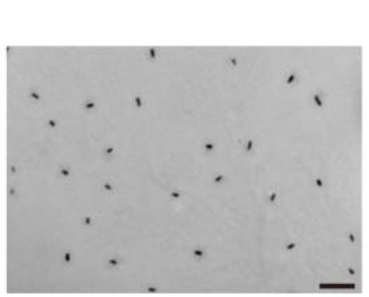

归一化UV-Vis光谱显示H4-PEG-PT在~800 nm处有最大吸收峰，在~1050 nm处有最大发射峰

透射电子显微镜测定，H4-聚乙二醇-PT在水中容易形成平均长度为180.0±13 nm，平均宽度为48±15 nm的超分子聚集体。

Introduction

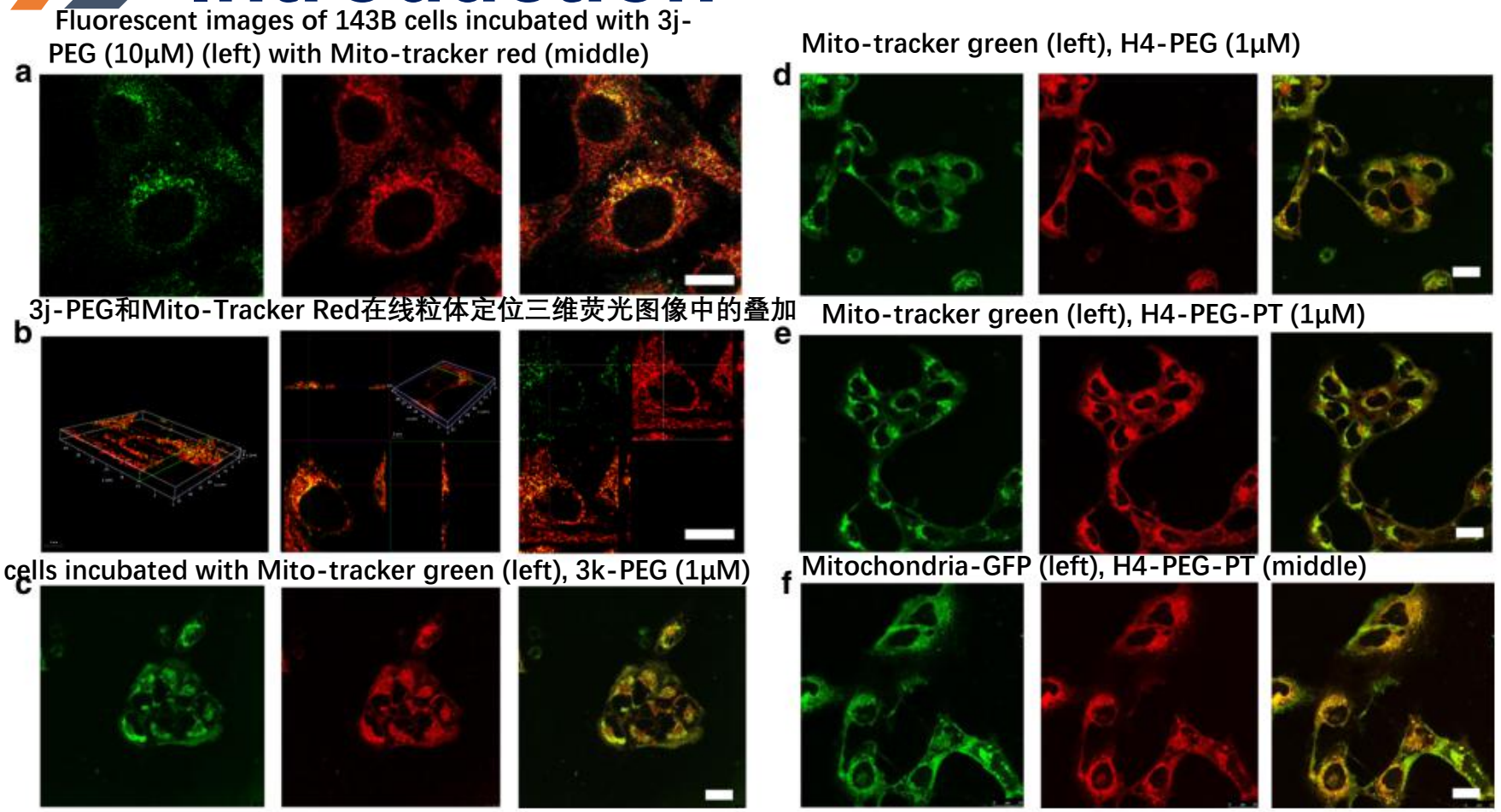

如图6a-e所示，所有不同浓度的3j-PEG、3k-PEG、H4-PEG或H4-PEG-PT的荧光图像都与商业线粒体染料(MTR或MTG)的荧光图像有较好的重叠，表明这些合成染料具有线粒体靶向能力。

NIR-II荧光共聚焦研究表明3J-PEG、3k-PEG、H4-PEG和H4-PEG-PT被跨越内膜的线粒体摄取，并通过离域的亲脂性阳离子硫代吡咯盐获得线粒体靶向。

Fig. 6 Mitochondrial localization. a Fluorescent images of 143B cells incubated with 3j-PEG (10 μM) for 8 h (left); with Mito-tracker red (middle) and merge images of them (right). λ_{em}: 590–650 nm, λ_{ex}: 594 nm (Mito-tracker red); λ_{em}: 490–540 nm, λ_{ex}: 488 nm (3j-PEG). **b** Merge images of 3j-PEG and Mito-tracker red in 3D fluorescence images of mitochondrial localization. **c–e** Fluorescent images of 143B cells incubated with Mito-tracker green (left), with **c** 3k-PEG (1 μM) or **d** H4-PEG (1 μM), or **e** H4-PEG-PT (1 μM) for 6 h (middle) and merge images them (right), respectively. λ_{em}: 495–526 nm, λ_{ex}: 488 nm (Mito-tracker green); λ_{em}: 610–660 nm, λ_{ex}: 514 nm (3k-PEG, H4-PEG, and H4-PEG-PT). **f** Fluorescent images of 143B cells incubated with Mitochondria-GFP (left), H4-PEG-PT (middle), and merge images of them (right). λ_{em}: 495–526 nm, λ_{ex}: 488 nm (Mitochondria-GFP); λ_{em}: 610–660 nm, λ_{ex}: 514 nm (H4-PEG-PT). Scale bar: 10 μm. Results in (**a–f**) are representative of three independent experiments.

Introduction

裸鼠原位143B肿瘤的X线与生物发光成像叠加(左)、裸鼠原位143B肿瘤的X线成像(中)

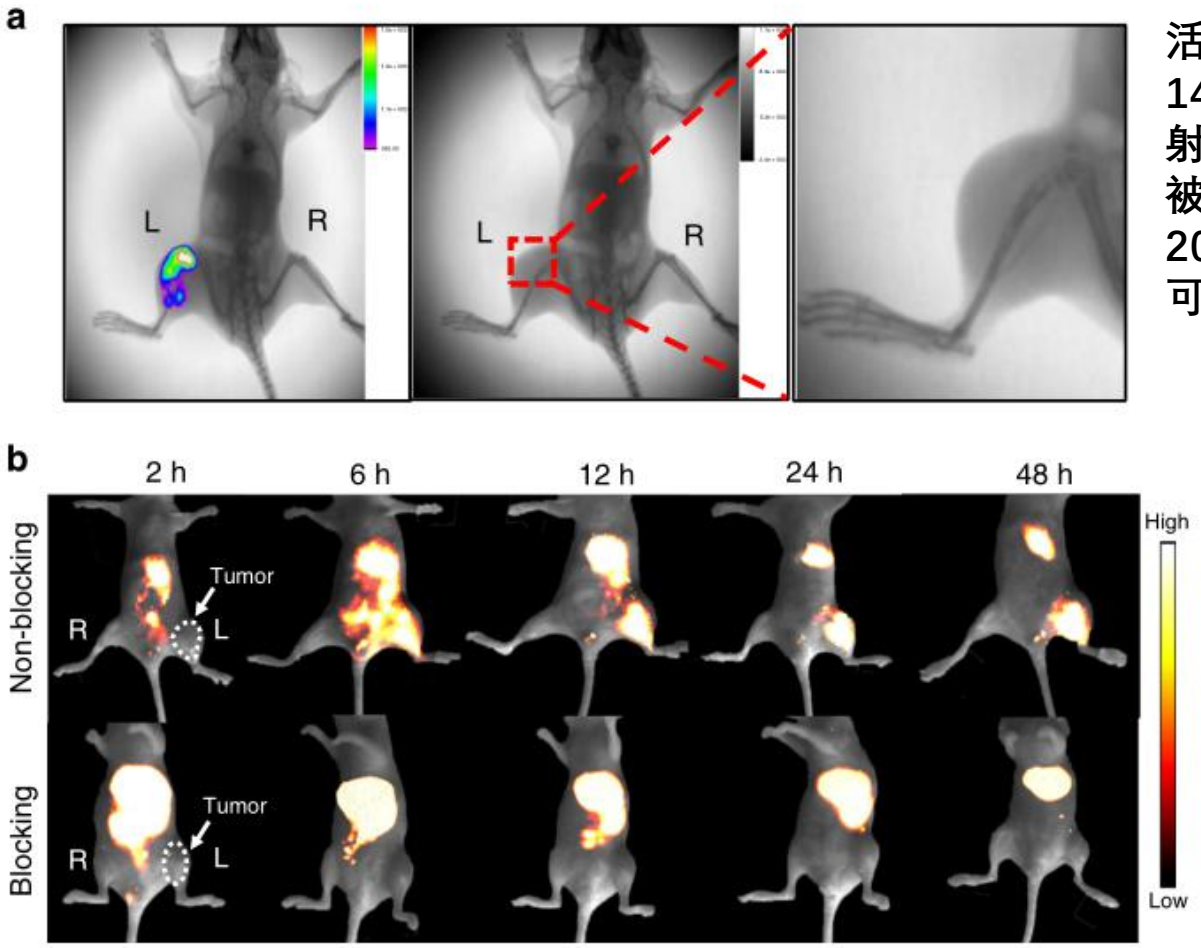

活体成像。通过原位注射绿色荧光蛋白(GFP)转染的143B细胞建立143B小鼠肿瘤模型。通过GFP发光和X射线成像监测原位肿瘤的生长，直到关节的胫骨近端被143B细胞吞噬然后静脉注射H4-PEG-PT(200μg，200μL)给143B荷瘤小鼠。从NIR-II成像中，从6~48h可清楚地将143B肿瘤与周围的背景组织区分开来。

与正常组比较，阻断组各时间点均可观察到较弱的荧光信号。阻断实验证实了H4-PEG-PT对骨肉瘤的靶向性。

Fig. 7 In vivo imaging of osteosarcoma. a Merge of X-ray and bioluminescence imaging of orthotopic 143B tumor in the nude mouse (left), X-ray imaging of orthotopic 143B tumor in the nude mouse (middle) and enlarged images of proximal tibia of the joint (right) (prone position) ($n = 3$ biologically independent mice). **b** NIR-II signals of H4-PEG-PT in 143B tumor mice (top) and the blocking group (bottom) under 808 nm excitation (1000 LP, 3.5 W, 250 ms) (supine position) ($n = 3$ biologically independent mice).

Introduction

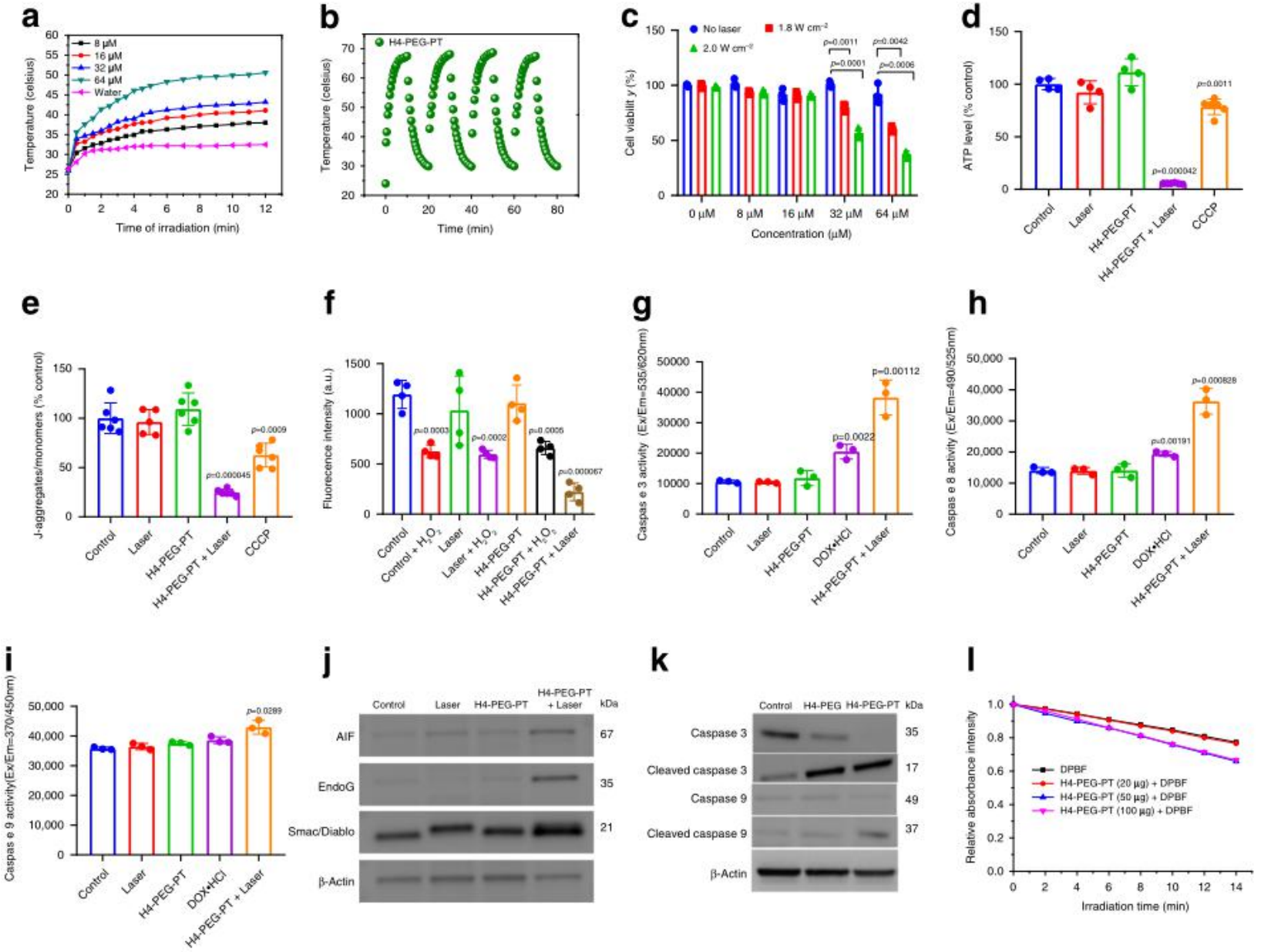

Introduction

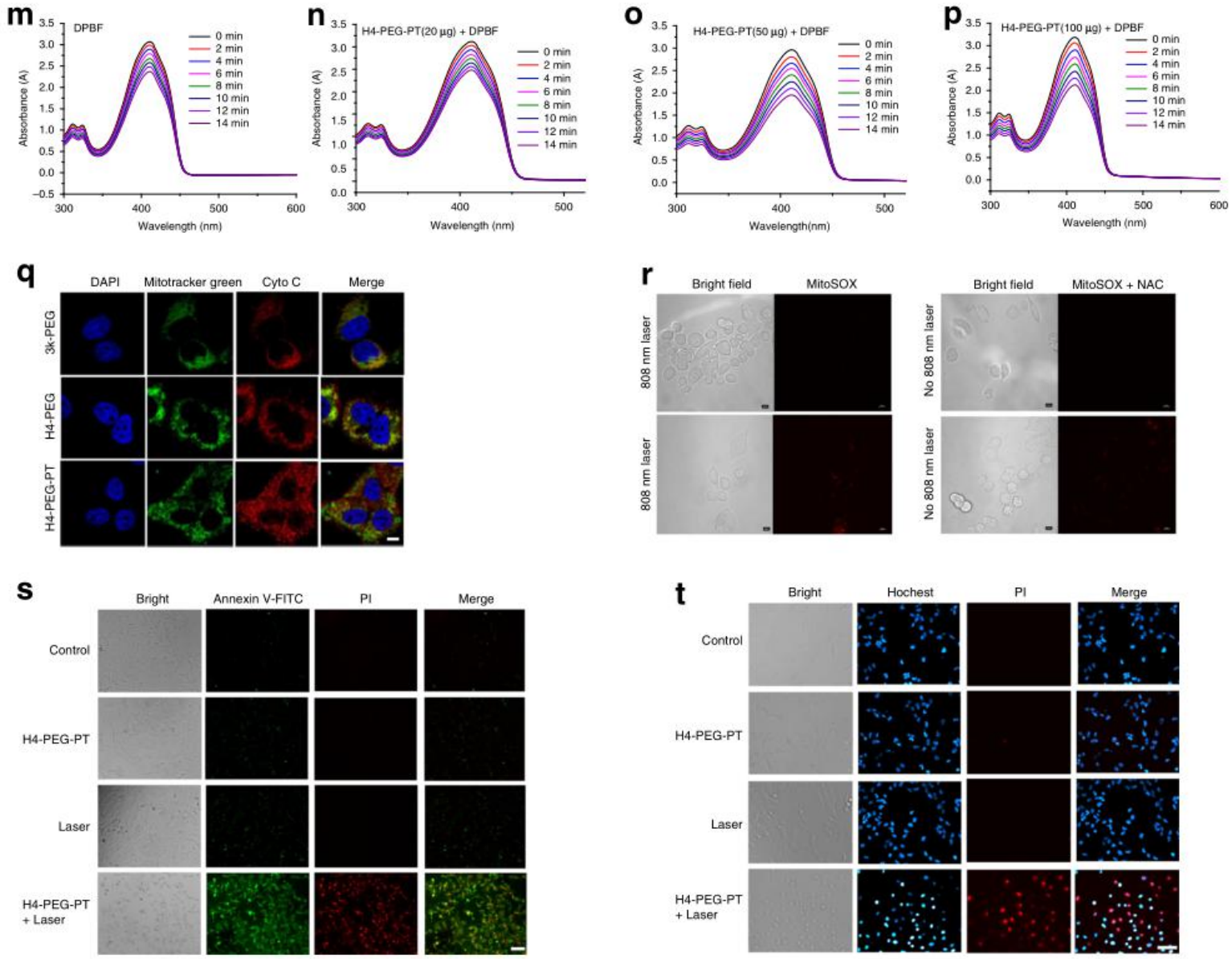

Introduction

研究了808 nm近红外激光对143B荷瘤小鼠体内光热治疗的影响

PBS solution injected

注射后，皮肤仅有轻微的温度升高

H4-PEG-PT solution

注射后，肿瘤表面温度在8分钟内从33.0℃迅速上升到67.8℃

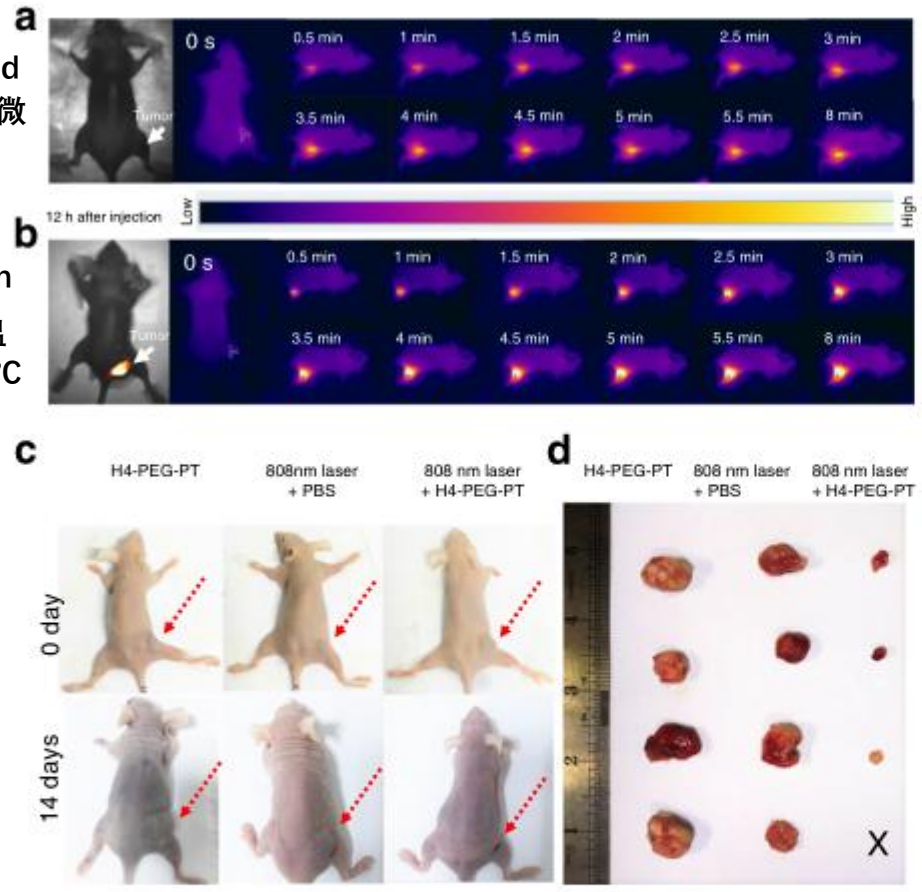

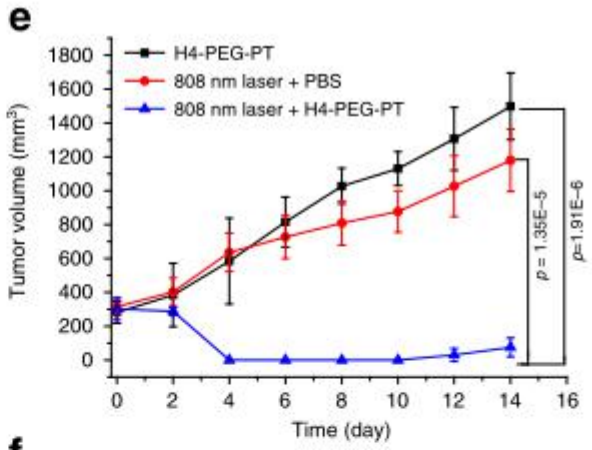

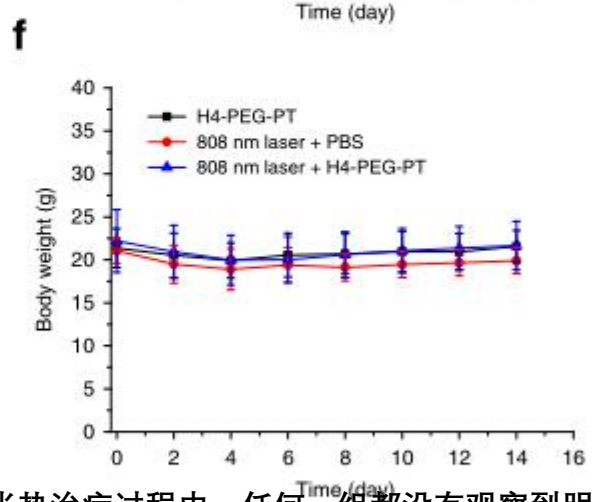

体内光热研究表明，H4-PEG-PT有效地将808 nm的激光转化为热量。

在光热治疗过程中，任何一组都没有观察到明显的体重减轻。

Fig. 9 In vivo photothermal evaluation of H4-PEG-PT against osteosarcoma. a PBS and **b** H4-PEG-PT solution injected to tumor bearing mice under 808 nm laser irradiation (1.5 W cm^{-2}). **c** Representative photographs of mice after different treatments: H4-PEG-PT only, PBS under 808 nm laser irradiation, and H4-PEG-PT exposed to 808 nm irradiation, respectively. Red dashed arrows indicated tumor. **d** Photographs of tumor tissue obtained in different groups after 14 d treatment, respectively. **e** Tumor volumes and **f** body weight of different groups of 143B tumor-bearing mice after treatment ($n = 4$ biologically independent mice). Data are presented as mean values ± SD (**e**, **f**). Statistical significance was calculated with two-tailed Student's *t* test (**e**).